1 *Article*

2 # A Hybrid Lagrangian-Eulerian Particle Model for

3 # Ecosystem Simulation

4 **Pengfei Xue [1,2]*, David J Schwab [3], Xing Zhou [1], Chenfu Huang [1], Ryan Kibler [1], Xinyu Ye [1]**

5 [1] Department of Civil and Environmental Engineering, Michigan Technological University, Houghton,
6   Michigan
7 [2] Great Lakes Research Center, Michigan Technological University, Houghton, Michigan
8 [3] Michigan Tech Research Institute, Michigan Technological University, Ann Arbor, Michigan
9 * Corresponding author: Dr. Pengfei Xue, Michigan Tech, 1400 Townsend Dr., Building GLRC-317,
10   Houghton, MI 49931; E-mail: pexue@mtu.edu

11 **Abstract:** Current numerical methods for simulating biophysical processes in aquatic
12 environments are typically constructed in a grid-based Eulerian framework or as an
13 individual-based model in a particle-based Lagrangian framework. Often, the biogeochemical
14 processes and physical (hydrodynamic) processes occur at different time and space scales, and
15 changes in biological processes do not affect the hydrodynamic conditions. Therefore, it is possible
16 to develop an alternative strategy to grid-based approaches for linking hydrodynamic and
17 biogeochemical models that can significantly improve computational efficiency for this type of
18 linked biophysical model. In this work, we utilize a new technique which links hydrodynamic
19 effects and biological processes through a property-carrying particle model (PCPM) in a
20 Lagrangian/Eulerian framework. The model is tested in idealized cases and its utility is
21 demonstrated in a practical application to Sandusky Bay. Results show the integration of
22 Lagrangian and Eulerian approaches allows for a natural coupling of mass transport (represented
23 by particle movements and random walk) and biological processes in water columns which is
24 described by a nutrient-phytoplankton-zooplankton-detritus (NPZD) biological model. This
25 method is far more efficient than traditional tracer based Eulerian biophysical models for 3-D
26 simulation, particularly for a large domain and/or ensemble simulations.

27 **Keywords:** Property-carrying Particle Model; coupled models; Ecosystem Simulation; Biophysical
28 Modeling; Sandusky Bay; Great Lakes

29 ## 1. Introduction

30   Current numerical methods for simulating biogeochemical processes in aquatic environments
31 are typically constructed as Individual-based models (IBMs) using Lagrangian particles [1-3] or as
32 grid-based concentration models in an Eulerian framework [4-6]. IBMs allow for a mechanistic
33 description of individuals and of interactions among individuals, represented by an ensemble of
34 particles. Each individual contains a set of state variables (e.g., age, size, and nutrient quota) with
35 corresponding physiological traits and behavioral traits [3], and the population-level properties
36 emerge as a result of the cumulative behavior of the individuals [7]. IBMs have rapidly gained
37 popularity in ecological modeling, particularly when simulating complete life cycles, adaptive
38 behavior, and intrapopulation variability in response to internal and external environmental
39 conditions becomes essential [8, 9]. Large computational demand has long been known as one of the
40 hallmark problems for IBM [2,7,8]. This is still true even with increased computational resources and
41 implementation of the strategic approaches for reducing the number of individuals explicitly
42 simulated in the model such as introducing the super individual particles or representative spaces
43 [2].
44   On the other hand, the traditional grid-based Eulerian approach is also widely used in the
45 coupled physical-biogeological modeling [6,7,10,11] in the inland water and ocean modeling
46 communities [12-18]. The Eulerian (concentration) model assumes average properties (state

47 variables) of a population within a control volume, and estimate the change of the property using
48 mass balance and reaction equations [19]. It does not describe intrapopulation variability but focuses
49 on characteristics of the population mean, which is appropriate when growth kinetics are
50 formulated as a function of the external conditions [7].
51   In general, the Eulerian model employs finite difference or finite element schemes to solve the
52 governing reaction-transport equations [4, 6]. Equations for the time evolution of state variables of
53 the biophysical model include advection and diffusion terms which depend on hydrodynamic
54 variables, as well as source and sink terms representing growth, decay, and interaction with other
55 biogeochemical variables [6,11,22]. The property concentration fields ($C_i, i = 1,2,3 ....$) are often
56 calculated using a set of advection-diffusion equations:

$$\frac{\partial DC_i}{\partial t} + \frac{\partial DuC_i}{\partial x} + \frac{\partial DvC_i}{\partial y} + \frac{\partial DwC_i}{\partial z} - \frac{1}{D}\frac{\partial}{\partial z}\left(K_h \frac{\partial C_i}{\partial z}\right) - DF_c = C_{i,source} - C_{i,sink} \qquad (1)$$

58 where D is the total water depth, $u, v,$ and w are the $x, y,$ and z components of the water velocity,
59 K_h is the vertical thermal diffusion coefficient, F_c is the horizontal diffusion term, and $C_{i,source}$ and
60 $C_{i,sink}$ represents the sources and sinks of C_i , respectively, due to the biological processes which are
61 typically described using a set of biological process equations.
62   However, even in the relatively simple, less computationally demanding Eulerian model, a
63 major practical challenge is that the biological submodel often involves a large group of parameters
64 for calibration and confirmation which requires a considerable amount of computational time to
65 tune the model. As shown in Equation 1, tuning the simulation of biological processes (e.g.,
66 changes in parameterization, initial and boundary conditions) requires a complete time integration
67 of the entire equation, although bio-physical coupled models can have different time steps for
68 physical and biological process terms as they may have different time and space scales. However,
69 biophysical processes are generally not two-way coupled. In other words, one can often assume that
70 changes in biological processes (in our case, the resulting changes in
71 nutrient-phytoplankton-zooplankton-detritus (NPZD) property concentration) do not affect the
72 hydrodynamic condition (currents, temperature, mixing, etc.). This indicates that there may be a
73 more computationally efficient approach to resolve the impact of hydrodynamics on the biological
74 processes rather than explicit integration of Equation 1 for each biological component every time the
75 biological submodel is tuned.
76   The property-carrying particle model (PCPM) is developed to test the feasibility of an
77 alternative strategy to grid-based approaches for linking hydrodynamic and biogeochemical models
78 in the Eulerian framework that may reduce the problems mentioned above, particularly in regions
79 where advection-diffusion plays a key role in regulating biogeochemcal processes. Instead of
80 grid-based, time-averaging of hydrodynamic variables, the hydrodynamic model is used to calculate
81 the Lagrangian trajectories of a large number of current-following tracer particles; these trajectories
82 become the linking mechanism between the hydrodynamic model and the biogeochemical model. In
83 the hybrid Lagrangian-Eulerian PCPM, each current-following tracer particle carries with it a
84 number of time-varying properties which correspond to the state variables of the Eulerian
85 biogeochemical model. The PCPM also employs its own horizontal grid system or series of regions
86 which is independent of the hydrodynamic model grid and is used to calculate local average values
87 of the particle-based properties. These cell-based properties allow all particles within a PCPM cell to
88 influence the properties of other particles within the same cell or region and allow for display and
89 analysis of biogeochemical fields. PCPM also differs from typical IBMs in that the tracer particles in
90 PCPM typically carry 'field' based properties like concentration, as opposed to properties associated
91 with an individual organism.
92   PCPM uses a computational grid system which is independent of the grid system used to
93 compute currents for particle trajectories. The PCPM computational cells are used to define regions
94 in which the properties carried by the particles are allowed to interact with one another. In this
95 respect, PCPM is conceptually similar to the classic Particle-in-Cell (PIC) method with PM
96 (particle-mesh) interactions [23, 24], popularly used in plasma simulation [24, 25]. PIC methods can
97 also be mesh-independent by allowing direct particle-particle (PP) interactions, or a combination of

98   PM and PP [23-26]. In PCPM, a basic simplifying assumption is that only particles within a single
99   PCPM cell are allowed to interact, such as the PIC-PM method. The advantage of this approach is
100 that it is conceptually intuitive to implement and computationally efficient to program.
101   An alternative approach to implementing a PCPM would allow particle-based properties to
102 influence particle trajectories, perhaps through buoyancy or sinking. In this case, the PCPM would
103 have to be directly coupled with the particle trajectory calculation. In the initial implementation of
104 PCPM in this paper, we consider only the uncoupled case.
105   To illustrate more clearly the type of application envisioned for PCPM, we constructed and
106 applied a rudimentary biophysical model to an actual aquatic system, Sandusky Bay, where the
107 physical transport of flow and nutrient loading from the Sandusky River has proven to be critical to
108 the ecosystem [27, 28]. Since the mid-1990s, harmful algal blooms (HABs) have become the new
109 norm for summer months in the Lake Erie ecosystem [29]. Harmful algal blooms occur in the system
110 when cyanobacteria are provided the right temperature, light, and nutrient conditions to proliferate
111 [28]. When these blooms transpire, they have many adverse impacts. At the local ecosystem level,
112 HABs result in depleted dissolved oxygen levels below the lake's surface threatening the survival of
113 organisms living below the surface [31]. Additionally, some cyanobacteria species produce a toxin,
114 such as microcystin, which affects the nervous system, liver, and kidney further impeding aquatic
115 organisms and humans [31].
116   "Whereas the colonial cyanobacterium Microcystis dominates the cHAB community in
117 offshore regions of western Lake Erie, filamentous Planktothrix has been shown to persist in
118 N-limited bays and tributaries" [28], such as in Sandusky Bay [27,28,32]. Situated on Lake Erie's
119 southwestern coast, Sandusky Bay borders Ohio's Ottawa, Erie, and Sandusky counties (Figure 1).
120 From a physical aspect, Sandusky Bay is relatively shallow bay with an average depth of roughly 2.6
121 meters as well as occupying a relatively small area [32]. The primary draining watershed to
122 Sandusky Bay is originates from the Sandusky River on the west end of the bay. The Sandusky River
123 drains a 1,420 square mile area; of which, over 80% is dedicated to agricultural production [31]. This
124 largely agricultural watershed leads to high nitrogen and phosphorus entering Sandusky Bay.
125 Combining these high nutrient loads with the physical aspects leads to very high concentrations of
126 nitrogen and phosphorus within Sandusky Bay, thus resulting in these cyanobacteria blooms
127 (Planktothrix *agardhii*) [27,28,32].
128   The intent of this study is to test the feasibility of PCPM for biological-physical coupled
129 modeling and examine its effectiveness and computational efficiency in practical application by
130 implementing it in relation to HABs in Sandusky Bay. The remaining sections of this paper are
131 organized as follows: Details of PCPM and the design of numerical experiments are described in
132 section 2. The model results of idealized cases and the practical application to Sandusky Bay are
133 presented in section 3. A discussion and summary of the PCPM applications are included in section
134 4.
135
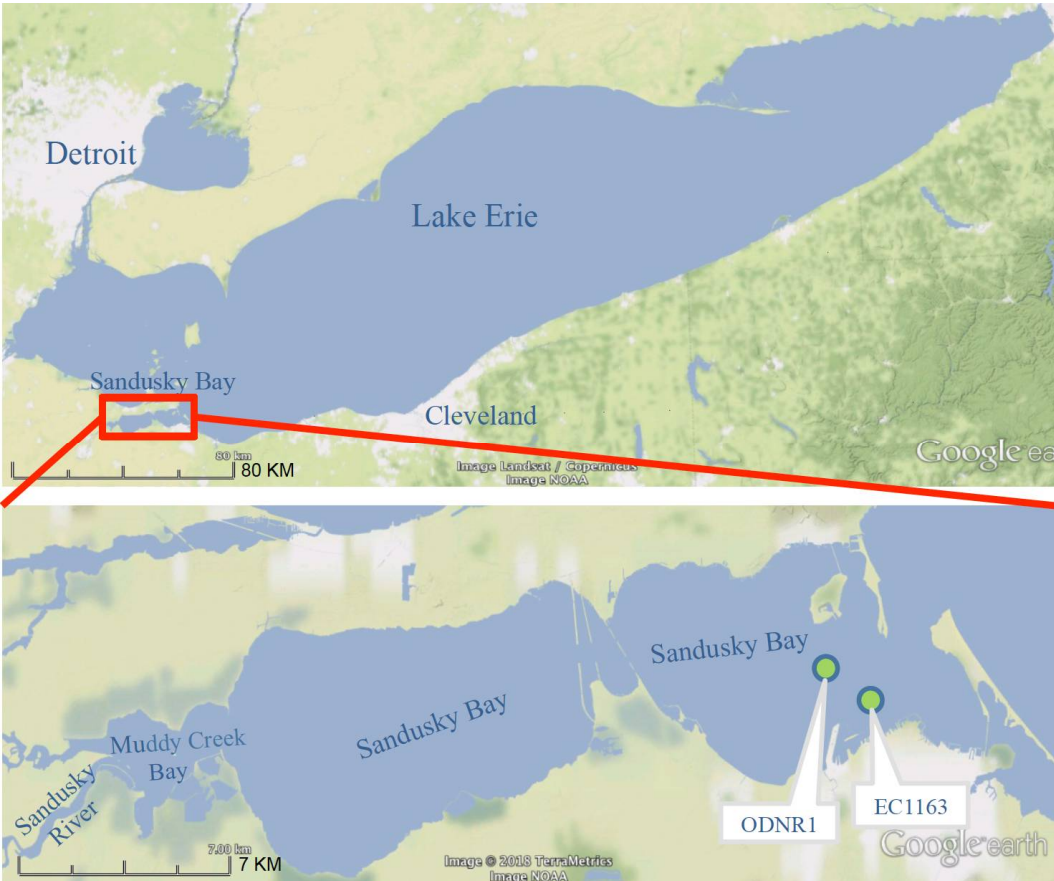
Figure 1.   Sandusky Bay is situated on Lake Erie's southwest coast occupying a small portion of the Great Lake's coastline. Sandusky Bay is relatively shallow bay with an average depth of ~2.6 meters. The primary draining watershed to Sandusky Bay originates from the Sandusky River on the west end of the bay. Sampling stations ODNR1 and EC1163 are denoted with green dots.

2. Methods

2.1 PCPM

In this implementation of PCPM, particle trajectories are pre-computed based on the output of a hydrodynamic model and are independent of the particle properties. An initial particle density (i.e., total number of particles / volume of computational domain) is selected and particles are randomly distributed throughout the computational domain. Particles are not allowed to leave the computational domain except at hydrodynamic outflows. At hydrodynamic inflows, new particles are introduced with the same density as the initial distribution. The total number of active particles is not strictly preserved, but if there is a net balance of hydrodynamic inflows and outflows, the total number of particles is approximately constant.

Any suitable method can be used to generate the Lagrangian particle trajectories. Typically, the trajectories are calculated from a time integration of the Lagrangian equations of motion:

$$\frac{dx}{dt} = u, \frac{dy}{dt} = v, \frac{dz}{dt} = w \tag{2}$$

where (x,y,z) is the particle's position in 3 dimensions, (u,v,w) is the local fluid velocity vector, and t is time. For the two idealized examples presented in this paper, the trajectories are calculated semi-analytically from a simple, idealized flow field. The third, more realistic example, demonstrates the use of a full hydrodynamic model of a natural basin (i.e., Sandusky Bay) to compute currents and trajectories.

Each computational time step in the PCPM consists of six intermediate steps:

1. Read particle locations (x, y, z) and temperature. This step simply updates the location of each particle that is being used in the computation. Figure 2 is a conceptual representation of a PCPM computational cell, Particles (m_1, m_2, m_3, …) move in and out of the cell at each PCPM time step based on their trajectories as computed from the hydrodynamic model. The total number of particles for a particular computation is assumed to be fixed for the duration of the computation, although some particles may enter or leave the PCPM domain during the computation. Water temperature or other physical properties from the hydrodynamic calculation can be stored along with the pre-computed particle trajectories and can be included as one of the properties ($P1$, $P2$, $P3$, …) carried by the particle.

2. Determine the PCPM cell for each particle. In Figure 2, the PCPM cell is represented by the enclosing rectangle. The PCPM domain need not coincide with the domain that was used for the hydrodynamic simulation and computation of particle trajectories. It can be regular or irregular, as long as there is a prescribed method to calculate which PCPM cell contains a prescribed particle position (x, y, z). The PCPM cells are the volumes within which particle properties can interact, that is, during a single time step, all particles within a PCPM cell can influence the evolution of particle properties within that cell, but are independent of other cells.

3. Apply boundary conditions to any particle-based properties that require them. If there is a property (e.g., concentration of a dissolved nutrient) that needs to be specified as a boundary condition, then particles within the cell where the boundary condition needs to be applied will have that property adjusted to meet the boundary condition. For example, in a cell that is associated with an inflow to the domain, the properties that are being carried into the domain through the inflow are adjusted to take account of the change in that property for particles within that cell. Alternatively, if particles from the hydrodynamic-based trajectory calculation are entering a PCPM cell, the values of the associated properties for each particle need to be specified.

4. Calculate PCPM cell-based averages of each property. In this step, the averages of K_{th} property for cell n are calculated as

$$\overline{PK_n} = \sum_{j=1}^{L} PK_{m_j}/L \tag{3}$$

where the summation includes all L particles (m_1, m_2,..m_L) currently within cell n. L is the number of particles within that cell. If no particles are present in a particular cell, PCPM uses the values of $\overline{PK_n}$ from the previous time step.

5. Calculate the time evolution of the cell-based properties (and particle-based properties if necessary) using the process equation defined for that property. The process equations can incorporate terms which depend on either particle-based or cell-based properties, or both, i.e.

$$\overline{PK_n(t + \Delta t)} = FN(P1_M(t), P2_M(t), P3_M(t), \dots \overline{P1_n}(t), \overline{P2_n}(t), \overline{P3_n}(t), \dots) \tag{4}$$

Note that M indicates m_1, m_2,..m_L. The form of *FN* is completely general and depends on the problem being solved. For instance, in a NPZD model, the Pi, ($i = 1,2,3 \dots$)would be N, P, Z, D, and water temperature, and the *FN* would be the process equations relating these properties.

Since the cell-based averages have already been computed, the right-hand side of equation 4 is independent of the left-hand side, so the computation of the evolution equations can be carried out in parallel. This is another key design feature of PCPM allowing it to take full advantage of multiprocessing computer environments, both Symmetric Multi-Processing (SMP) and Massively Parallel Processing (MPP).

6. Redistribute cell-based properties to particles within each cell by replacing the particle-based property with a weighted average of the cell-based property. After the evolution equations have been carried out (Step 5), particles within an individual cell most likely carry a range of different values of the various properties, which vary around the new cell-based average computed in Step 5, $\overline{PK_n(t + \Delta t)}$. PCPM provides an optional step to reduce the variance of the new particle-based properties within each cell. This optional step is applied as a 'nudging' term, i.e.

213
$$PK_m(t + \Delta t) = (1 - \alpha_i)PK_m(t) + \alpha_i \overline{PK_n(t + \Delta t)} \qquad (5)$$

214   where $0 < \alpha_i < 1$ is the redistribution weight (i.e. nudging) factor. If $\alpha_i = 0$, no adjustment is carried
215   out and particle-based property remain unchanged. If $\alpha_i = 1$, then all particles within a cell are
216   assigned the cell-based average of that property. This step can be useful to smooth results
217   when limited particle density results in excessive within-cell variability.

218
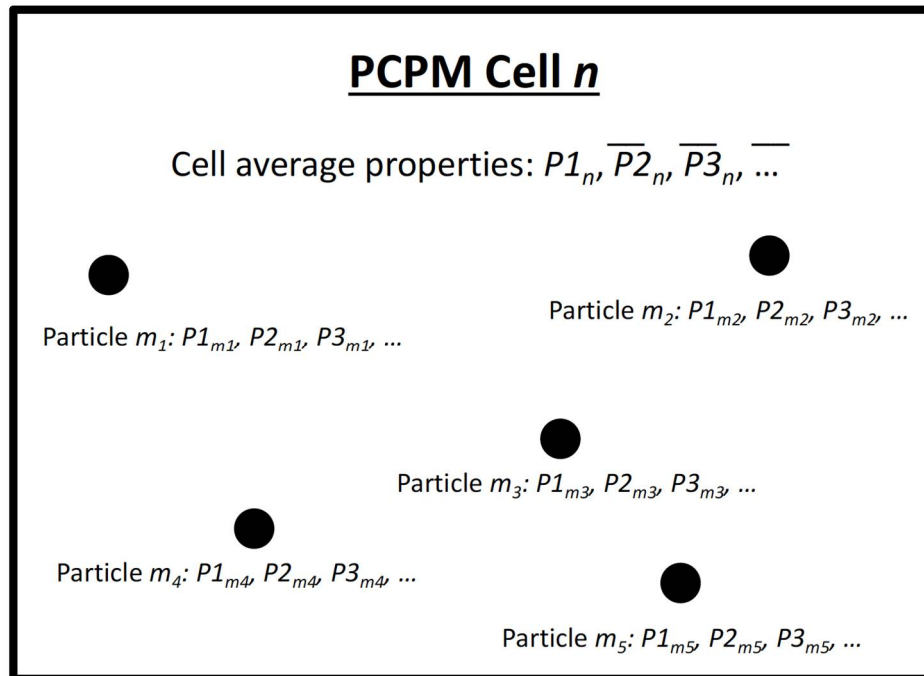
219   **Figure** 2. Conceptual representation of a PCPM computational cell n and particles (m_1, m_2, m_3, m_4,
220   m_5...) within the cell n. PCPM cell-based average of each property ($\overline{P1_n}$, $\overline{P2_n}$, $\overline{P3_n}$,...) is determined
221   by the property values carried by the particles that have entered in this cell. After time evolution of
222   PCPM properties using process equations, the updated PCPM cell-based properties ($\overline{P1_n}$, $\overline{P2_n}$,
223   $\overline{P3_n}$,...) are redistributed to particles with a weighted average. Then the particles move around
224   carrying the updated properties to different PCPM computational cell in the next cycle.

225   Note that all steps except 3 and 5 are independent of the specific problem, i.e., they will be
226   carried out the same way no matter how many properties are attached to the particles or what
227   those properties represent. More importantly, steps 1 and 2 only need to be run once regardless
228   of modifications in biological processes at the later stage. These are two of the key designs of
229   PCPM that contribute to enhanced computational efficiency.

230   *2.2 Idealized Case 1: Advection-diffusion plume*

231   In PCPM, diffusion is provided mainly by particle trajectories, although the cell-based
232   averaging of particle properties and the (optional) redistribution of cell-based properties to
233   particles within the cell can also act as diffusive terms. To demonstrate the effect of particle
234   trajectory diffusion on particle properties, we constructed a 500 m wide x 2000 m long channel
235   divided into 10 m square cells. Particles were introduced at random locations along the center
236   400 m section of the left edge of the channel at the rate of 100/sec. The particles were assigned an
237   along-channel velocity of 2 m/sec. Horizontal diffusion was added using a random-walk
238   perturbation to the particle trajectories of $2r\sqrt{2k_h\Delta t}$ in both cross-channel and long-channel
239   directions. Here, r is a uniformly distributed random number in the range [-1,1], k_h is the
240   horizontal diffusion coefficient (10 m²/sec in this experiment), and Δt is the time step for the
241   particle trajectory calculation (1 sec).

242   In this example, PCPM particles carry only one property, concentration (P1=C), and there is no
243   time evolution equation (step 5, above). The purpose of this example is to illustrate how PCPM
244   simulates horizontal diffusion through a combination of the particle trajectories and the
245   cell-based averaging in step 6. To simulate a concentration plume, particles introduced in the
246   center of the left wall (-50 m < y < 50 m) are assigned the initial condition C = 1. Particles
247   entering the channel outside this region have an initial condition of C = 0.

248   *2.3 . Idealized Case 2: Vertical settling*

249   Since this implementation of PCPM does not allow the properties carried by the particles to
250   influence particle trajectories, the question arises of how to simulate the vertical transport of a
251   property when the vertical transport depends on the property itself, such as sediment settling or
252   biologically generated buoyancy. In PCPM, the answer is simply to solve the vertical transport at the
253   PCPM cell-based Eulerian framework in step 5 as a traditional cell-based method. Interaction of
254   particle properties with adjacent cell averages is technically not allowed in the basic PCPM
255   framework, but an exception is made in this case. The vertical advection-diffusion equation for
256   sediment concentration is shown below

257
$$\frac{\partial C}{\partial t} = w_s \frac{\partial C}{\partial z} + k_z \frac{\partial^2 C}{\partial z^2} \tag{6}$$

258   where w_s is the bulk settling velocity of the suspended material and k_z is the vertical diffusion
259   coefficient.
260   Since vertical diffusion is already included in the particle trajectories, PCPM only needs to
261   consider the first term on the right-hand side of (7) to account for the additional vertical transport
262   that depends on the property itself. To implement this term in PCPM, the process equation for a
263   particle carrying a property C_m in vertical cell k looks like

264
$$C_m(t + \Delta t) = C_m(t) + w_s \Delta t \left(\overline{C_{k-1}(t)} - \overline{C_k(t)} \right) \Delta z + (other\ process\ terms) \tag{7}$$

265   where $\overline{C_k(t)}$ is the average concentration in vertical cell k, $\overline{C_{k-1}(t)}$ is the average concentration in
266   the next higher vertical cell, and Δz is the spacing between the centers of the cells. For particles in
267   the top cell (k=0), we set

268
$$C_m(t + \Delta t) = C_m(t) - w_s \Delta t \overline{C_0(t)} \Delta z + (other\ process\ terms) \tag{8}$$

269   and for particles in the bottom cell (k=$kmax$), we set

270
$$C_m(t + \Delta t) = C_m(t) - w_s \Delta t \overline{C_{kmax}(t)} \Delta z + (other\ process\ terms) \tag{9}$$

271   As a test case, we examine the vertical settling in a one-dimensional water column of depth d with
272   particles moving vertically only through vertical diffusion. Particles are initially distributed
273   randomly in the column and then move with a random walk velocity of $2r\sqrt{2k_z\Delta t}$ where r is a
274   uniformly distributed random number in the range [-1,1] and k_z is the vertical diffusion coefficient.
275   Particles are not allowed to cross the surface or bottom boundaries. Thus, in this experiment, the
276   number of particles is constant and the particles are always approximately uniformly distributed in
277   the vertical due to vertical mixing.
278   For the experiment, we set $C = 1$ as the bottom boundary condition by assigning this value at
279   the beginning of each time step to all particles in the lower half of the bottom cell. The initial
280   condition in other cells is $C = 0$. For the test case, we set the number of particles to 1000, $d = 20$ m, k_z
281   = 10^{-4} m^{2}s^{-1}, and the redistribution parameter $\alpha = 0.1$. Three runs were made with 5, 10, and 20 vertical
282   cells respectively. PCPM is integrated in time with $\Delta t = 1$ hr.

283   *2.4 Sandusky Bay Model*

284   The hydrodynamic model used in this study is FVCOM (Finite Volume Community Ocean
285   Model) [33]. FVCOM is an unstructured-grid, finite-volume, three-dimensional (3-D) primitive

equation ocean model with a generalized, terrain-following coordinate system in the vertical and a triangular mesh in the horizontal. The unstructured grid can be designed to provide a customized variable resolution to both coastline and bathymetry. With the merits of ideal geometric fitting and local refinement of mesh resolution, FVCOM has been used in numerous applications to estuaries, coastal oceans, and the Great Lakes [34-40]. These characteristics make the model well suited for the study of Sandusky Bay.

Although this study focuses on Sandusky Bay, FVCOM is configured to simulate physical dynamics for all of Lake Erie, thus providing reliable representation of large-scale background circulation and the role of remote forcing impacting the water movement in the bay through the opening; additionally, this configuration avoids the impact of setting an artificial numerical boundary condition for our target region. The hydrodynamic model is well-calibrated for the Lake Erie, based on the next-generation NOAA Lake Erie Operational Forecast System [LEOFS; see Kelley et al., [40] for detailed model validation], a real-time nowcast and forecast model that is built on the FVCOM. In the upgraded NOAA operational model for Lake Erie [40], the FVCOM model is developed with horizontal resolution ranging from 100 to 2500 meters, and 21 uniform vertical sigma (terrain-following) layers for Lake Erie. The advantage of our model setting is that model resolution varies from 100-2500 m (coarse) in the open lake to 10-50 m (fine) in Sandusky Bay, affording a high degree of resolution across the 20 km x 3 km study site and adequately resolving the geographic complexity and coastal hydrodynamic conditions of that system (Figure 3). The model configuration yields a total of 73,000 grid elements (cells) in the horizontal plane with 50,000 of them resolving the bay.

In the PCPM implementation, 86,000 initial particles are randomly distributed throughout Sandusky Bay with a total water volume of 3.01×10^8 m^3. With PCPM cell resolution of 200 x 200 m and the mean water depth of 2.6 m in Sandusky Bay, each PCPM cell contains 30 particles on average. New particles are introduced from the Sandusky River with the same density as the initial distribution. The number of new particles released from the river mouth varies greatly in accordance with the river flow rate. Table 1 presents the number of new particles released each month, based on the total water volume input from the Sandusky River. For example, 205,367 particles are released in March due to the highest river discharge in this month, which approximately equals the total number of particles (207,050) released from April to October.

Table 1. The number of new particles released and the total water volume input from the Sandusky River in each month.

Month	Monthly Discharge (10^8 m^3)	Particles(number)
Jan	0.364	10,405
Feb	2.27	64,980
Mar	7.19	205,367
Apr	1.53	43,741
May	0.443	12,640
Jun	3.00	85,754
Jul	1.97	56,347
Aug	0.129	3,680
Sep	0.089	2,544
Oct	0.093	2,654
Nov	0.133	3,798
Dec	1.15	32,951

334
335

Figure 3. FVCOM model mesh for Lake Erie (upper panel) and linked with a high-resolution mesh for Sandusky Bay (lower panel). Only a portion of the Sandusky Bay mesh is displayed for a clear representation of the mesh's resolution.

2.5 Sandusky Bay Biological Model

The biological model used in this work is a general 3-D NPZD model [17]. As a common approach, the biological model is constructed by implementing 1-D NPZD models for each vertical column of PCPM cells that are distributed spatially across the 2-D domain to form a 3-D representation of the system. Exchange of properties between adjacent water columns occurs across their shared interface through advection and dispersion. Figure 4 displays the interactions among state variables in the NPZD model.

$$\begin{cases} \frac{dN}{dt} - \frac{\partial}{\partial z}\left(K_h \frac{\partial N}{\partial z}\right) - F_Z = -P(uptake) + Z(respiration) + P(respiration) + D(remineralization) \\ \frac{dP}{dt} - \frac{\partial}{\partial z}\left(K_h \frac{\partial P}{\partial z}\right) - F_P = P(uptake) - P(respiration) - P(mortality) - ZP(grazing) + P(sinking) \\ \frac{dZ}{dt} - \frac{\partial}{\partial z}\left(K_h \frac{\partial Z}{\partial z}\right) - F_Z = ZP(grazing) + ZD(grazing) - Z(respiration) - Z(mortality) \\ \frac{dD}{dt} - \frac{\partial}{\partial z}\left(K_h \frac{\partial D}{\partial z}\right) - F_D = P(mortality) + Z(mortality) - ZD(grazing) - D(remineralization) + D(sinking) \end{cases} \quad (10)$$
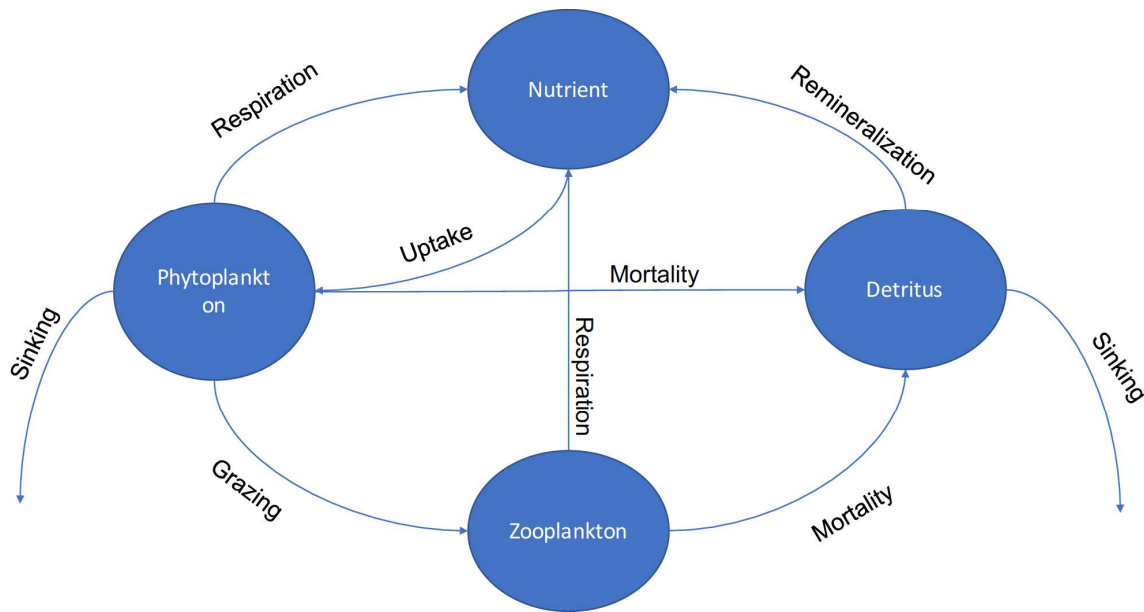
Fig. 4. A schematic representation of the NPZD model.

The governing equations for the model framework are based on Luo et al. [17], and the mathematical expressions for each term of the system of equations 10 is presented in Appendix A. Several equations in the governing equations are modified for this study based on literature review. The light-limited, nutrient-limited, and temperature-limited functions $f(I), f(N), f(T)$, respectively, that contribute to the $P(uptake)$ are taken from Platt et al. [41] and Nicklisch et al. [42]. Also, the light attenuation functions are adjusted to Rowe et al. [18].

$$f(I) = (1 - e^{-\frac{\alpha_I I}{\mu_{max}}})e^{-\frac{\beta_I I}{\mu_{max}}} \tag{11}$$

$$f(N) = \frac{N - N_0}{K_s + N - N_0} \tag{12}$$

$$f(T) = \exp(-2.3(\frac{T_{opt} - T}{T_{opt} - T_{min}})^2) \tag{13}$$

$$I = I_0 \exp(-k_d h) \tag{14}$$

where α_I, β_I are the initial linear slope at low irradiance and the negative slope at the high irradiance that characterizes photoinhibition [43], μ_{max} is the maximum potential growth rate, and I is the light intensity. The nutrient threshold N_0 represents the pool of nutrient that was assumed to be biologically unavailable. T_{opt} and T_{min} are the optimal growth temperature and minimal growth temperature, respectively. k_d is the light attenuation coefficient that accounts for the impact of water turbidity, phytoplankton, and detritus on the light attenuation. Model parameterization is based on literature review [17,18,41,43] and subjective tuning for the Sandusky Bay simulation as there is no established NPZD model for the Sandusky Bay region. (See Table 2 for model parameterization).

3. Results

3.1. Idealized Case 1: Advection-diffusion plume

To illustrate the effect of the cell-based averaging (step 6), we show results of the first idealized case for four different values of the cell-based redistribution parameter (α = 0, 0.01, 0.1, 0.5) in Figure 5. In Figure 5, there are three panels for each value of α. The top panel shows the locations of particles after 720 time steps (12 minutes). The particles are colored using a blue-to-red scale for

375 concentration values from 0 to 1. Particles with a concentration value of exactly 0 are colored light
376 gray. The second panel shows the average concentration in each 10 m square cell with the same blue
377 to red scale as the top panel, except cells with C = 0 are black. The third panel compares
378 concentration along the centerline of the plume from the second panel to the analytical solution for a
379 diffusive plume [44,45], i.e.,

380
$$C(x) = \mathrm{erf}([\tfrac{2}{3}([1.4x + 1]^{0.833} - 1)]^{-0.5}) \tag{15}$$

381 where $C(x)$ is the centerline concentration x meters away from the channel entrance. In the case
382 $\alpha = 0$, there is no cell-based redistribution of properties, so all particles retain their initial
383 concentration values of either C=0 (light gray in panel 1) or C=1 (red in panel 1). As seen in the
384 second and third panels, the random-walk diffusion in the particle trajectories does provide a rough
385 approximation to the analytical solution by mixing of C=0 and C=1 particles in PCPM cells. Of course
386 increasing the number of particles in the simulation would provide a more accurate approximation,
387 but would also increase the computational load. Setting the cell-based redistribution parameter to
388 even the small value of α = 0.01 provides a significant improvement in the solution with the same
389 number of particles, particularly for x > 500 m. Now particles can have any value of C between 0 and
390 1. Increasing the redistribution parameter to α = 0.1 further improves the solution for x < 500 m.
391 Further increasing α to 0.5 does not significantly improve the solution in comparison to α = 0.1.
392
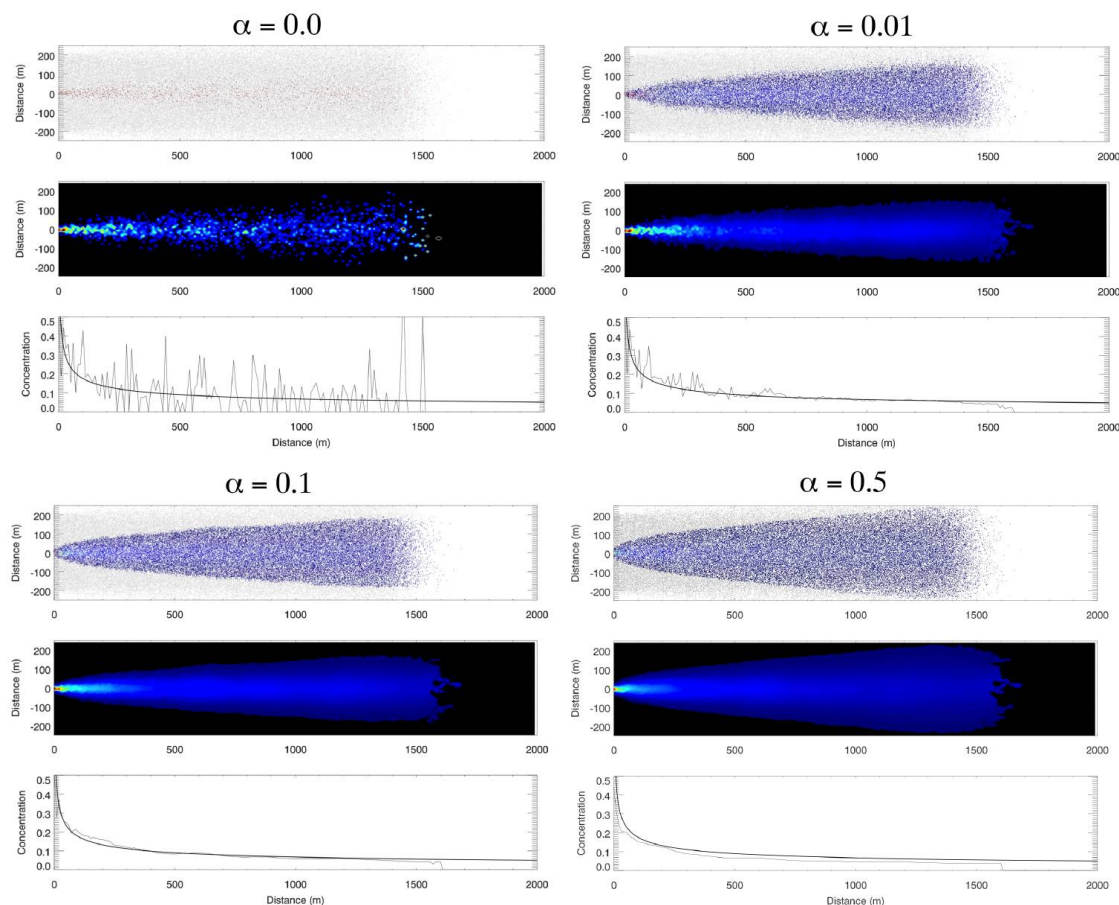
393
394 **Figure 5.** PCPM simulation of concentration plume in an idealized channel with four different values
395 of the cell-based redistribution weight parameter (α = 0, 0.01, 0.1, 0.5). There are three panels for each
396 value of α. The top panel shows the locations of particles after 720 time steps (12 minutes). The
397 second panel shows the average concentration in each 10 m square cell with the same blue to red
398 scale as the top panel, except cells with C = 0 are black. The third panel compares concentration along
399 the centerline of the plume from the second panel to the analytical solution for a diffusive plume.

3.2. Idealized Case 2: Vertical settling

The results at the end of 5,000 time steps of the second idealized case are shown in Figure 6. In Figure 6, the dots represent the locations of the particles on the vertical axis and the value of concentration they are carrying on the horizontal axis. The thin line is the cell average concentration. The thick line is the analytical solution,

$$C = e^{\frac{-w_s}{k_z}z} \tag{11}$$

As shown in Figure 6, the model properly simulates the change in concentration due to vertical settling and mixing while allows the particles to remain approximately uniformly distributed in the vertical.   The simulation accuracy increases with increased resolution of vertical layers. The model result with 20 vertical layers shows a close agreement with the analytical solution. Specifically, Figure 7 shows the evolution in time of the root mean square difference (RMSD) between the cell averages and the analytical solution for the three cases. While the RMSD in the simulation with 5 layers remains above 0.2 (the magnitude of initial error) over the entire simulation, the RMSD decreases quickly to 0.02 after 500 time steps and remains stable at this level when vertical resolution is increased to 20 layers.
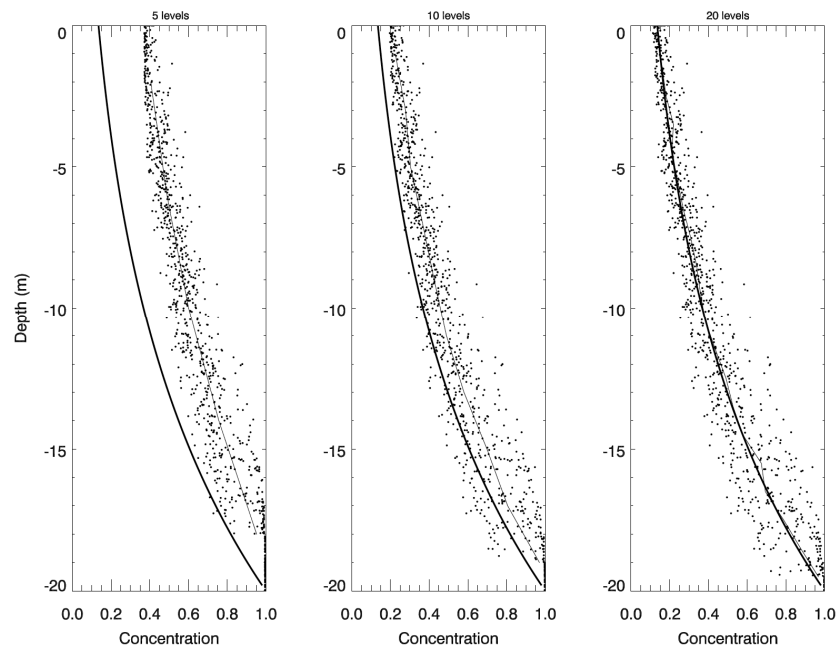
Figure 6. The PCPM simulation of vertical settling in comparison to the analytical solution at the end of 5,000 time steps. Three runs were made with 5, 10, and 20 vertical cells, respectively. The dots represent the locations of the particles on the vertical axis with their respective concentration on the horizontal axis. The thin line represents the cell average concentration and the thick line represents the analytical solution.

421
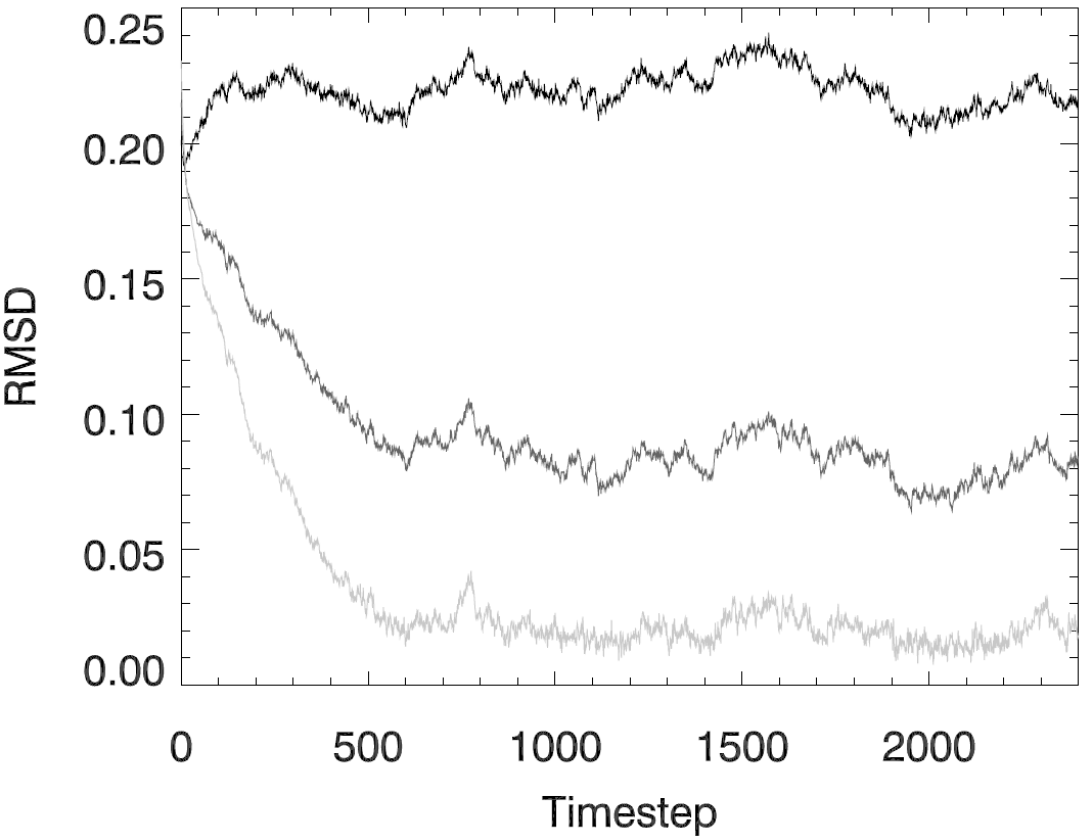
Figure 7. The time evolution of the root mean square difference (RMSD) between the cell averages and the analytical solution for the three cases presented in the Figure 3 (dark line for 5 cells, medium line for 10 cells, and light line for 20 cells).

3.3 Application to Sandusky Bay

To ensure the validity of the 1-D NPZD biological model, it was configured to duplicate several scenarios (not shown) from Edwards et al. [46]. The model demonstrated the expected linear stability of a vertically-distributed, NPZ ecosystem model when it was used in the scenarios that incorporate the impact of vertical mixing on biological dynamics. Scenarios include stable profiles, damping oscillatory dynamical trajectories, and vertically phase-locked systems, depending on the depth and choice of parameters and strength of vertical diffusion, which can be discerned from the eigenvalues in linear stability analysis [46]. The 1-D NPZD model used in this study reproduced all of these cases almost identically.

Before examining the impact of physical transport on the biological dynamics in Sandusky Bay, we first tested the ability of PCPM to simulate the advection-diffusion of a passive tracer in a natural setting. The Sandusky river plume is simulated using the conventional soluble-tracer model based on Equation 1 and compared to the PCPM model approach in Figure 8. It is clear that the plumes simulated using the two methods show a very similar pattern, indicating the validity of the PCPM. Upon closer review, the plume simulated with soluble-tracer model shows a smoother evolution and sharper gradient near the plume front. We speculate this is partly due to the constant random-walk scale (10 m^2/s) used in the current particle-tracking model configuration. Nonetheless, the attractiveness of PCPM is its computational efficiency; it runs ~100 times faster than the soluble-tracer model which will be discussed in detail in the following section and table 2.

444
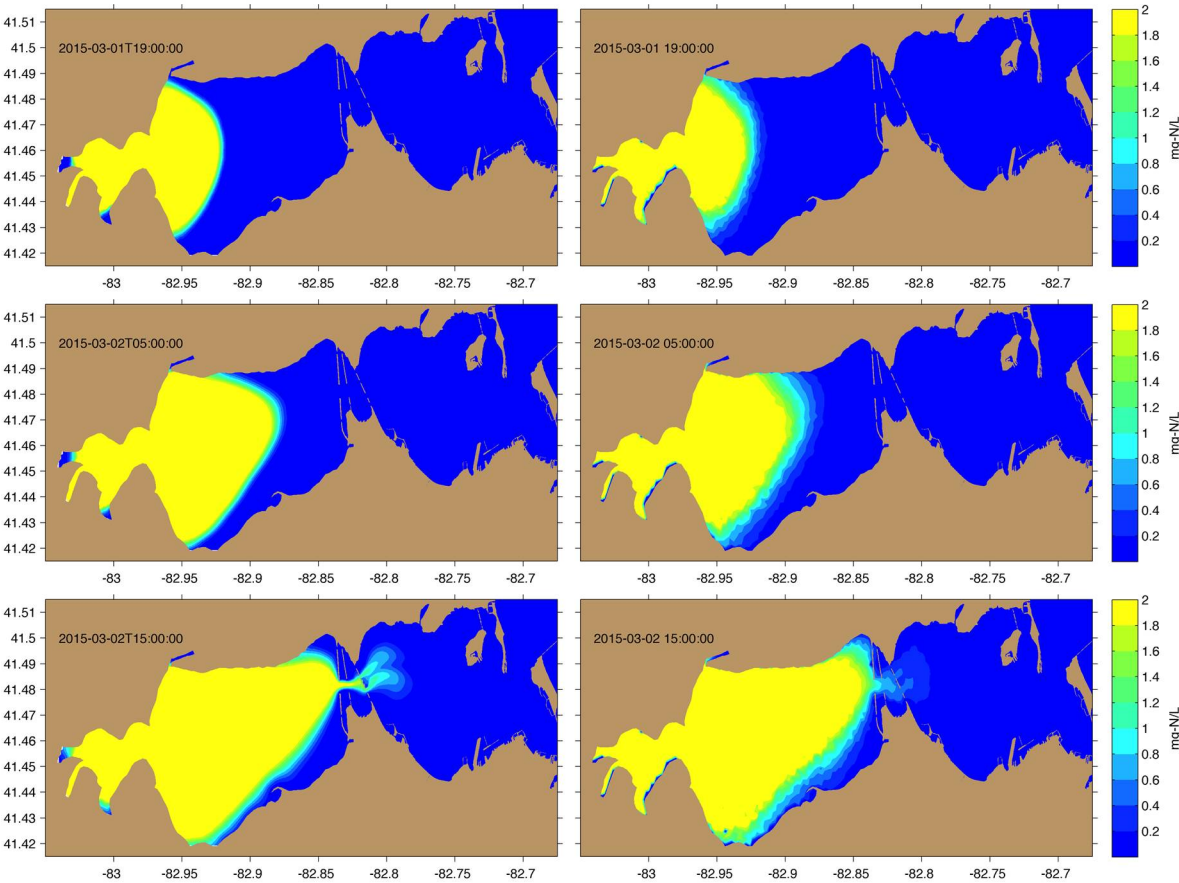
Figure 8.   River plumes simulated with conventional soluble-tracer model (left panels) and PCPM
model (right panels). The color scale represents the nitrogen concentration.

447   To aid in model development, several datasets are gathered from literature as well as data
448   acquisition organizations. Sandusky River daily discharge and nitrogen concentration are available
449   from the National Center for Water Quality Research (https://ncwqr.org/monitoring/data/).
450   Nitrogen, Chlorophyll concentration, and in-situ temperature data are available from two
451   observational sites (ODNR1 and EC1163) in the eastern bay from May – October 2015, sampled by
452   Bowling Green State University [28].
453   Using the PCPM-NPZD model, the importance of physical transport is demonstrated by
454   comparing model results between the PCPM-NPZD-NOADV simulation and the realistic
455   PCPM-NPZD-REAL simulation. In the PCPM-NPZD-NOADV simulation, the model is configured
456   the same as the PCPM-NPZD-REAL, except the movement of particles is driven only by turbulent
457   diffusion without including advective processes due to the Sandusky River and wind field. Each
458   simulation consists of three cases that use a high initial nutrient concentration of 9 mg N/L in June
459   (case 1), medium initial concentration of 0.46 mg N/L averaged from July to September (case 2), and
460   low initial concentration of 0.0075 mg N/L in August (case 3), respectively. The concentration values
461   are estimated as total nutrient loading from the Sandusky River to the Bay
462   (https://ncwqr.org/monitoring/data/) divided by the total water volume of the bay. The comparison
463   of model results is presented in Figure 9. The simulation of PCPM-NPZD-NOADV without
464   resolving the advective transport processes shows a significant discrepancy from observational data
465   (Figure 9, upper panels). The model fails to capture both the timing and magnitude of the blooms in
466   all three cases, and model results are sensitive to the initial nutrient concentration.
467   On the other hand, after the impact of advective processes is resolved in the
468   PCPM-NPZD-REAL simulation, the model accurately depicts the magnitude of the chlorophyll peak
469   in mid-August (Figure 9, lower panels), and model results are insensitive to the initial condition, but
470   determined by Sandusky River discharge and its nutrient loading. Three cases show nearly
471   indentical results. Results also support the field sampling study in Salk et al. [28]. Their study finds a

472   strong, nonlinear connection between the bloom occurrence and the hydraulic residence time of the
473   bay, which varies dramatically from 8 days to several months depending on the Sandusky River
474   flow rate in the physical transport process. Although further development of the NPZD is
475   undoubtedly necessary to resolve the onset and variability of the algal blooms by refining the
476   structure of the biological model and improve the model parameterization, it is beyond the scope of
477   this work, in which we focus on demonstrating the feasibility of linking hydrodynamic effects and
478   biological processes through the PCPM in a Lagrangian/Eulerian framework. Further development
479   of the biological model and its application to the study of mechanisms responsible for the HABs in
480   Sandusky Bay will be presented in another paper.

481
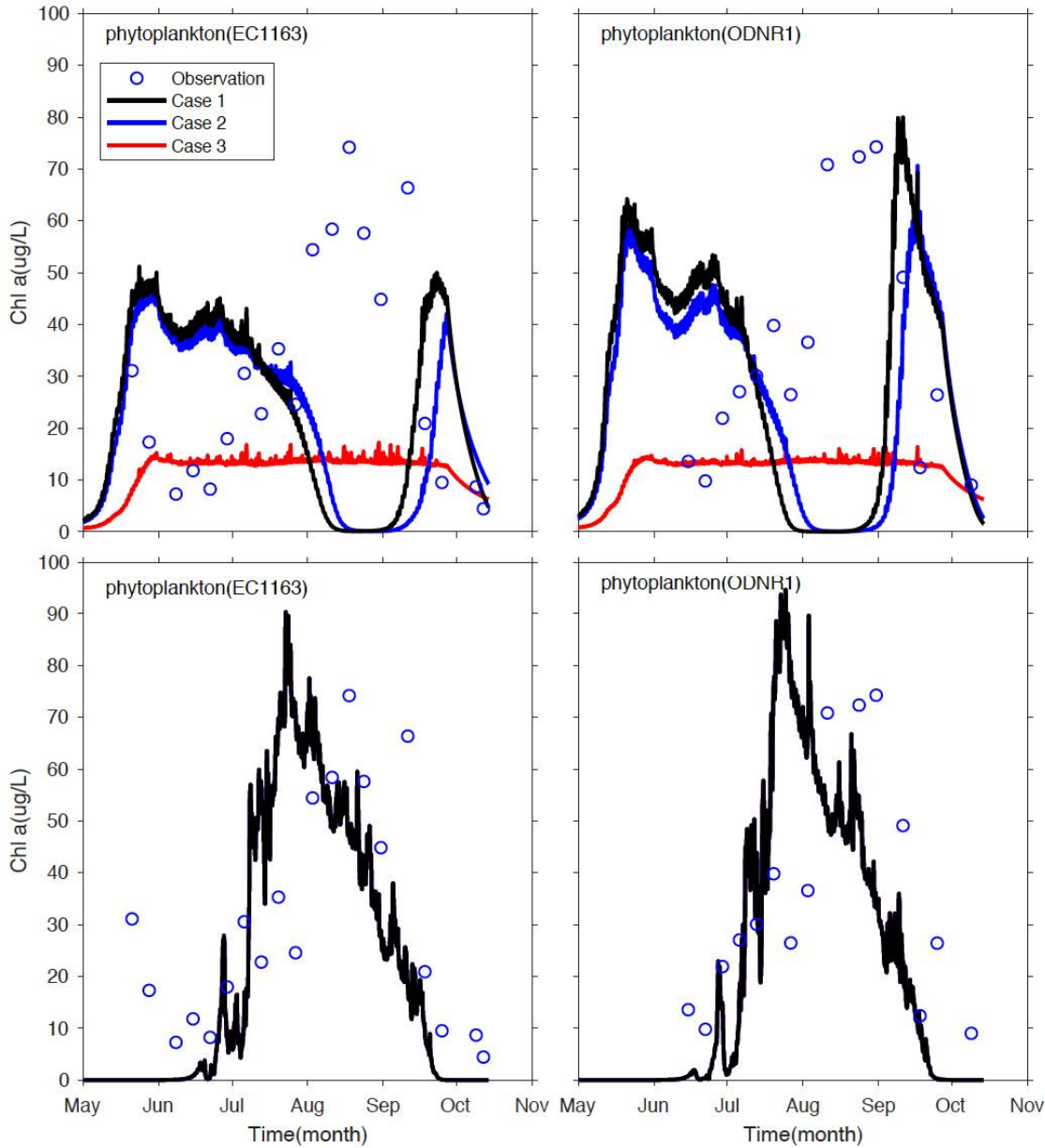
482   **Figure** 9. Observed and model simulated Chlorophyll concentration at the sampling stations EC1163
483   and ODNR1. The upper panels are results from the PCPM-NPZD-NOADV model simulations; the
484   lower panel are the results from the realistic PCPM-NPZD model simulations where the three cases
485   show nearly identical results, so only one result is plotted.

5. Summary and Conclusions

487   In this paper, we describe a novel method by integrating a property-carrying particle model
488   (PCPM) and an Eulerian concentration biological model for ecosystem modeling. The model is

489 tested in idealized cases and its utility is demonstrated in a practical application to Sandusky Bay.
490 The novelty of this new technique lies in its integration of hydrodynamic effects via the
491 property-carrying particle tracking model and Eulerian grid-based biological modeling approach.
492 Overall, there are several advantages of the PCPM over traditional Eulerian-based tracer
493 approaches. The PCPM is simpler to implement and more efficient as it does not need to solve the
494 advection-diffusion equation. Instead, the PCPM uses pre-computed particle trajectories to resolve
495 the hydrodynamic condition based on currents from a hydrodynamic model. This means that the
496 hydrodynamic model only needs to be run once giving one the ability to run different biological
497 scenarios for the same physical characteristics; ultimately saving significant computational time.
498   As summarized in Table 2, a 30-day hydrodynamic simulation for the Lake Erie-Sandusky Bay
499 FVCOM model takes 15 hours to complete using 64 CPUs. This step is necessary for both the
500 PCPM-NPZD model and the traditional Eulerian, grid-based biophysical model. Once the
501 hydrodynamic simulation is complete, PCPM-NPZD requires to calculate the Lagrangian
502 trajectories of a large number of current-following tracer particles; it takes 1.5 hours using single
503 CPU to track ~290,000 particles in the domain in March, which tracks the largest number of particles
504 in the bay within a single month. The PCPM-NPZD model simulation using the particle trajectories
505 as input completes a 30-day simulation within 5 minutes using a single CPU while it takes 5 hours
506 for traditional Eulerian, grid-based biophysical model to complete the same simulation using 32
507 CPUs. If compared with the same computational power (e.g., single CPU), the PCPM-NPZD
508 approach runs ~100 times faster for the biophysical modeling (Table 2; Scenario 1).
509   More importantly, in the PCPM framework, the hydrodynamics and associated water transport
510 and mixing represented by particle trajectories are "reserved" and not affected by biochemical
511 properties. In other words, it only takes another 5 minutes to run the PCPM-NPZD for a different set
512 of parameters and property configurations. This is extremely useful during the model calibration
513 and or ensemble simulations. The PCPM-NPZD would take 11.5 hours to complete 100 runs using a
514 single CPU, while traditional method would require 500 hours simulation using 32 CPUs (Table 2;
515 Scenario 2). Such a high level of efficiency is not available from tracer-based models because one will
516 have to re-run the Eulerian-based biological model for any change in parameter configuration or
517 estimation of different property concentration. Also, the PCPM is capable of providing comparable
518 simulation results to the soluble-tracer model, although the global and local mass conservation is not
519 strictly preserved with finite particles. Above all, it is the PCPM's computational efficiency and
520 coupling flexibility which makes it an attractive alternative method to the traditional approach.

526   **Table 2.** The comparison of total run time using the method developed in this study (new
527 method) and the grid-based Eulerian method (traditional method) in two scenarios. Scenario 1:
528 Conduct coupled biophysical model only once; Scenario 2: Run ensemble simulation of the coupled
529 biophysical model for 100 simulations with different biological parameterization.
530

	Simulation period (day)	# of CPUs	Time per run (hour)	Scenario 1		Scenario 2	
				Required runs	Total Time	Required runs	Total Time
Hydrodynamic simulation (required for both methods)	30	64	15	1	15 hrs	1	15 hrs

Biological simulation							
New Method							
Particle trajectory model	30	1	1.5	1	1.6 hrs (1 CPU)	1	11.5 hrs (1 CPU)
PCPM-NPZD	30	1	0.1	1		100	
Traditional Method							
Eulerian, grid-based simulation	30	32	5	1	5 hrs (32 CPUs)	100	500 hrs (32 CPUs)

531
532

533 **Appendix A. Biological Model Formulation and Parameters; the original value of the parameters**
534 **is provided in ( ) if tuned value was used.**

Parameters	Description	Units	Value used	References
k_s	Half-Saturation constant	µmol N/L	3 (0.6)	[17]
No	Nutrient threshold	µmol N/L	0 (1.4)	[18]
α_I	Initial linear slope at low irradiances	$\dfrac{mgC \cdot m^2}{mgChl \cdot Einst}$	7	[18]
β_I	Negative slope at high irradiances	$\dfrac{mgC \cdot m^2}{mgChl \cdot Einst}$	0	[43]
u_{max}	Maximum potential growth rate	$\dfrac{mgC}{mgChl \cdot h}$	2.4	[43]
T_{opt}	Optimum temperature	℃	27.2	[42]
T_{min}	Minimum temperature	℃	5.5	[42]
$u_{p(max)}$	Maximum growth rate for P	day^{-1}	1.1	
γ_p	Phytoplankton respiration coefficient	day^{-1}	0.01	[17]
γ_T	Exponential for Temperature forcing	dimensionless	0.07	[17]
γ_d	Remineralization rate of detritus	day^{-1}	0.015	[17]
G_{max}	Maximum P grazing rate by Z	day^{-1}	0.4	[17]
σ_P	Preference coefficient of Z on P	$(mmol\ C\ m^{-3})^{-1}$	0.5	[17]
σ_D	Preference coefficient of Z on D	$(mmol\ C\ m^{-3})^{-1}$	0.1	[17]
ϵ_p	Mortality rate of P	day^{-1}	0.005(0.01)	[17]

ϵ_Z	Mortality rate of Z	day $^{-1}$	0.2 (0.01)	[17]
W_P	Sink velocity of P	m/day	0.6	[17]
W_D	Sink velocity of D	m/day	0.6	[17]
a_w	Water attenuation coefficient	m $^{-1}$	0.07	[18]
a_p	Phytoplankton attenuation coefficient	$mgChl^{-1}m^2$	0.03	[18]
a_d	Detritus attenuation coefficient	g $detritus\ C^{-1}m^2$	0.2	[18]

535 The mathematical expressions for the biological terms in the system of equations (10) are listed
536 below, where the definition and value of each parameter in the equations is above.

$$P(uptake) = u_{p(max)} \cdot f(T) \cdot f(I) \cdot f(N) \cdot P \tag{A1}$$

$$P(respiration) = \gamma_p \cdot P \cdot exp(\gamma_T \cdot T) \tag{A2}$$

$$Z(respiration) = \gamma_z \cdot Z exp(\gamma_T \cdot T) \tag{A3}$$

$$D(remineralization) = \gamma_d \cdot D \cdot exp(\gamma_T \cdot T) \tag{A4}$$

$$ZP(grazing) = G_{max} \frac{\sigma_P P}{1 + \sigma_P P + \sigma_D D} Z \tag{A5}$$

$$ZD(grazing) = G_{max} \frac{\sigma_D D}{1 + \sigma_P P + \sigma_D D} Z \tag{A6}$$

$$P(mortality) = \epsilon_p P^2 \tag{A7}$$

$$Z(mortality) = \epsilon_z Z \tag{A8}$$

$$P(sinking) = -W_P \frac{\partial P}{\partial Z} \tag{A9}$$

$$D(sinking) = -W_D \frac{\partial D}{\partial Z} \tag{A10}$$

$$f(I) = (1 - e^{-\frac{\alpha_I I}{\mu_{max}}}) e^{-\frac{\beta_I I}{\mu_{max}}} \tag{A11}$$

$$f(N) = \frac{N - N_0}{K_s + N - N_0} \tag{A12}$$

$$f(T) = \exp(-2.3 (\frac{T_{opt} - T}{T_{opt} - T_{min}})^2) \tag{A13}$$

$$I = I_0 \exp(-k_d h) \tag{A14}$$

$$k_d = a_w + a_p P_{chl} + a_d D \tag{A15}$$

Author Contributions: Conceptualization, Pengfei Xue and David Schwab; Formal analysis, Xing Zhou, Chenfu Huang and Xinyu Ye; Project administration, Pengfei Xue; Validation, Xing Zhou; Visualization, Xing Zhou, Chenfu Huang and Xinyu Ye; Writing – original draft, Pengfei Xue and David Schwab; Writing – review & editing, Pengfei Xue, David Schwab.

Funding: This work is partly supported by the National Oceanic and Atmospheric Administration, grant# NA17NOS4780186.

Acknowledgments: This is the contribution XX of the Great Lakes Research Center at Michigan Technological University.

Conflicts of Interest: The authors declare no conflict of interest.

562

563   References

1.   Woods, J. D. (2005). The Lagrangian Ensemble metamodel for simulating plankton ecosystems. *Progress in Oceanography*, *67*(1-2), 84-159.

2.   Hellweger, F. L., & Bucci, V. (2009). A bunch of tiny individuals—Individual-based modeling for microbes. *Ecological Modelling*, *220*(1), 8-22.

3.   DeAngelis, D. L., & Grimm, V. (2014). Individual-based models in ecology after four decades. *F1000prime reports*, *6*.

4.   Chapra, S.C., 1997. Surface Water-Quality Modeling. McGraw-Hill, Boston.

5.   Franks, P. J. (2002). NPZ models of plankton dynamics: their construction, coupling to physics, and application. *Journal of Oceanography*, *58*(2), 379-387.

6.   Butenschön, M., Clark, J., Aldridge, J. N., Allen, J. I., Artioli, Y., Blackford, J., ... & Lessin, G. (2016). ERSEM 15.06: a generic model for marine biogeochemistry and the ecosystem dynamics of the lower trophic levels. *Geoscientific Model Development*, *9*(4), 1293-1339.

7.   Hellweger, F. L., & Kianirad, E. (2007). Individual-based modeling of phytoplankton: evaluating approaches for applying the cell quota model. *Journal of theoretical biology*, *249*(3), 554-565.

8.   Hellweger, F. L., Kravchuk, E. S., Novotny, V., & Gladyshev, M. I. (2008). Agent-based modeling of the complex life cycle of a cyanobacterium (Anabaena) in a shallow reservoir. *Limnology and Oceanography*, *53*(4), 1227-1241.

9.   Grimm, Volker, Uta Berger, Donald L. DeAngelis, J. Gary Polhill, Jarl Giske, and Steven F. Railsback. "The ODD protocol: a review and first update." *Ecological modelling* 221, no. 23 (2010): 2760-2768.

10. Bruggeman, J., & Bolding, K. (2014). A general framework for aquatic biogeochemical models. *Environmental modelling & software*, *61*, 249-265.

11. Chai, F., Dugdale, R. C., Peng, T. H., Wilkerson, F. P., & Barber, R. T. (2002). One-dimensional ecosystem model of the equatorial Pacific upwelling system. Part I: model development and silicon and nitrogen cycle. *Deep Sea Research Part II: Topical Studies in Oceanography*, *49*(13-14), 2713-2745.

12. Fennel, K., Wilkin, J., Levin, J., Moisan, J., O'Reilly, J., & Haidvogel, D. (2006). Nitrogen cycling in the Middle Atlantic Bight: Results from a three-dimensional model and implications for the North Atlantic nitrogen budget. *Global Biogeochemical Cycles*, *20*(3).

13. Edwards, K. P., Barciela, R., & Butenschon, M. (2012). Validation of the NEMO-ERSEM operational ecosystem model for the North West European Continental Shelf. *Ocean Science*, *8*, 983-1000.

14. Rodrigues, M., Oliveira, A., Queiroga, H., Fortunato, A. B., & Zhang, Y. J. (2009). Three-dimensional modeling of the lower trophic levels in the Ria de Aveiro (Portugal). *Ecological Modelling*, *220*(9-10), 1274-1290.

15. Xue, P., Chen, C., Qi, J., Beardsley, R. C., Tian, R., Zhao, L., & Lin, H. (2014). Mechanism studies of seasonal variability of dissolved oxygen in Mass Bay: A multi-scale FVCOM/UG-RCA application. *Journal of Marine Systems*, *131*, 102-119.

16. Chao, X., Jia, Y., Shields Jr, F. D., Wang, S. S., & Cooper, C. M. (2010). Three-dimensional numerical simulation of water quality and sediment-associated processes with application to a Mississippi Delta lake. *Journal of environmental management*, *91*(7), 1456-1466.

17. Luo, L., Wang, J., Schwab, D. J., Vanderploeg, H., Leshkevich, G., Bai, X., ... & Wang, D. (2012). Simulating the 1998 spring bloom in Lake Michigan using a coupled physical-biological model. *Journal of Geophysical Research: Oceans*, *117*(C10).

18. Rowe, M. D., Anderson, E. J., Vanderploeg, H. A., Pothoven, S. A., Elgin, A. K., Wang, J., & Yousef, F. (2017). Influence of invasive quagga mussels, phosphorus loads, and climate on spatial and temporal patterns of productivity in Lake Michigan: A biophysical modeling study. *Limnology and Oceanography*, *62*(6), 2629-2649.

19. Zhang, X.Y., 1995. Ocean outfall modeling – interfacing near and far field models with particle tracking method, PhD thesis, MIT.

20. Wong, K. T., Lee, J. H., & Choi, K. W. (2008). A deterministic Lagrangian particle separation-based method for advective-diffusion problems. *Communications in Nonlinear Science and Numerical Simulation*, *13*(10), 2071-2090.

21. Dimou, K. N., & Adams, E. E. (1993). A random-walk, particle tracking model for well-mixed estuaries

and coastal waters. *Estuarine, Coastal and Shelf Science, 37*(1), 99-110.

22. Xue, P., Schwab, D. J., Sawtell, R. W., Sayers, M. J., Shuchman, R. A., & Fahnenstiel, G. L. (2017). A particle-tracking technique for spatial and temporal interpolation of satellite images applied to Lake Superior chlorophyll measurements. *Journal of Great Lakes Research, 43*(3), 1-13.

23. Harlow, F.H. (1964). The Particle-in-Cell Computing Method for Fluid Dynamics. Methods in Computational Physics, 3, 319-343.

24. Tskhakaya D. (2008) The Particle-in-Cell Method. In: Fehske H., Schneider R., Weiße A. (eds) Computational Many-Particle Physics. Lecture Notes in Physics, vol 739. Springer, Berlin, Heidelberg

25. Hockney, R. W., and Eastwood, J. W. (1981). Computer Simulation Using Particles. McGraw-Hill, New York.

26. Grigoryev, Y.N., V.A. Vshivkov, and M.P. Fedoruk (2002). Numerical "Particle-in-Cell" Methods: Theory and Applications. De Gruyter VSP, Utrecht, Boston, 249pp.

27. Conroy, J. D., Kane, D. D., Quinlan, E. L., Edwards, W. J., & Culver, D. A. (2017). Abiotic and biotic controls of phytoplankton biomass dynamics in a freshwater tributary, estuary, and large lake ecosystem: Sandusky Bay (Lake Erie) chemostat. *Inland Waters*, *7*(4), 473-492.

28. Salk, K. R., Bullerjahn, G. S., McKay, R. M. L., Chaffin, J. D., & Ostrom, N. E. (2018). Nitrogen cycling in Sandusky Bay, Lake Erie: oscillations between strong and weak export and implications for harmful algal blooms. *Biogeosciences*, *15*(9), 2891.

29. Stumpf, R. P., Wynne, T. T., Baker, D. B., & Fahnenstiel, G. L. (2012). Interannual variability of cyanobacterial blooms in Lake Erie. *PloS one*, *7*(8), e42444.

30. Chaffin, J. D., Bridgeman, T. B., & Bade, D. L. (2013). Nitrogen constrains the growth of late summer cyanobacterial blooms in Lake Erie. *Advances in Microbiology*, *3*(06), 16.

31. U.S. EPA. (2017, Aug 10). *U.S. Action Plan for Lake Erie.* Retrieved from https://www.epa.gov/sites/production/files/2017/08/documents/us_dap_preliminary_draft_for_public_engagement_8-10-17.pdf

32. Davis, T. W., Bullerjahn, G. S., Tuttle, T., McKay, R. M., & Watson, S. B. (2015). Effects of increasing nitrogen and phosphorus concentrations on phytoplankton community growth and toxicity during Planktothrix blooms in Sandusky Bay, Lake Erie. *Environmental science & technology*, *49*(12), 7197-7207.

33. Chen, C., Liu, H., & Beardsley, R. C. (2003). An unstructured grid, finite-volume, three-dimensional, primitive equations ocean model: application to coastal ocean and estuaries. *Journal of atmospheric and oceanic technology*, *20*(1), 159-186.

34. Yang, Z., Wang, T., & Copping, A. E. (2013). Modeling tidal stream energy extraction and its effects on transport processes in a tidal channel and bay system using a three-dimensional coastal ocean model. Renewable Energy, 50, 605-613.

35. Xue, P., Schwab, D. J., & Hu, S. (2015). An investigation of the thermal response to meteorological forcing in a hydrodynamic model of Lake Superior. Journal of Geophysical Research: Oceans, 120(7), 5233-5253.

36. Anderson, E. J., Bechle, A. J., Wu, C. H., Schwab, D. J., Mann, G. E., & Lombardy, K. A. (2015). Reconstruction of a meteotsunami in L ake E rie on 27 M ay 2012: Roles of atmospheric conditions on hydrodynamic response in enclosed basins. Journal of Geophysical Research: Oceans, 120(12), 8020-8038.

37. Xue, P., J. S. Pal, X. Ye, J. D. Lenters, C. Huang, and P. Y. Chu (2017), Improving the Simulation of Large Lakes in Regional Climate Modeling: Two-Way Lake–Atmosphere Coupling with a 3D Hydrodynamic Model of the Great Lakes, *J. Climate, 30*, 1605-1627.

38. Khangaonkar, T., Nugraha, A., Xu, W., Long, W., Bianucci, L., Ahmed, A., ... & Pelletier, G. (2018). Analysis of Hypoxia and Sensitivity to Nutrient Pollution in Salish Sea. Journal of Geophysical Research: Oceans.

39. Ye, X., E. J. Anderson, P. Y. Chu, C. Huang, and P. Xue (2018). Impact of water mixing and ice formation on deep, inland lake warming: a model-guided mechanism study. Limnology and Oceanography, (accepted)

40. Kelley, J. G. W., Y. Chen, E. J. Anderson, G. A. Lang, and J. Xu, 2018. Upgrade of NOS Lake Erie Operational Forecast System (LEOFS) To FVCOM: Model Development and Hindcast Skill Assessment. NOAA Technical Memorandum NOS CS 40, 92 pp.

41. Platt, T. G. C. L., Gallegos, C. L., & Harrison, W. G. (1980). Photoinhibition of photosynthesis in natural

assemblages of marine phytoplankton.

42.   Nicklisch, A., Shatwell, T., & Köhler, J. (2007). Analysis and modelling of the interactive effects of temperature and light on phytoplankton growth and relevance for the spring bloom. *Journal of Plankton Research*, *30*(1), 75-91.

43.   Fahnenstiel, G. L., Chandler, J. F., Carrick, H. J., & Scavia, D. (1989). Photosynthetic characteristics of phytoplankton communities in Lakes Huron and Michigan: PI parameters and end-products. *Journal of Great Lakes Research*, *15*(3), 394-407.

44.   Stacey, M.T., E.A. Cowen, T.M. Powell, E. Dobbins, S.G. Monismith, and J.R. Koseff (2000). Plume dispersion in a stratified, near-coastal flow: measurements and modeling. Continental Shelf Research, 20, 637-663.

45.   Kim, T. and T. Khangaonkar (2012). An offline unstructured biogeochemical model (UBM) for complex estuarine and coastal environments. Environmental Modeling and Software, 31, 47-63.

46.   Edwards, C. A., Powell, T. A., & Batchelder, H. P. (2000). The stability of an NPZ model subject to realistic levels of vertical mixing. *Journal of Marine Research*, *58*(1), 37-60.

564